Available online at www.sciencedirect.com

ScienceDirect

journal homepage: www.elsevier.com/locate/nanoenergy

nano energy

RAPID COMMUNICATION

Si boride-coated Si nanoparticles with improved thermal oxidation resistance

Tae Kyoung Kim[a,d], Jaeyun Moon[a,d], Bryan VanSaders[a,b,d],
Dongwon Chun[a,d], Calvin J. Gardner[a,d], Jae-Young Jung[a,d],
Gang Wang[c], Renkun Chen[a,d], Zhaowei Liu[b],
Yu Qiao[c], Sungho Jin[a,d,*]

[a]Materials Science & Engineering, University of California at San Diego, 9500 Gilman Dr., La Jolla, CA 92093, USA
[b]Electrical & Computer Engineering, University of California at San Diego, 9500 Gilman Dr., La Jolla, CA 92093, USA
[c]Structural Engineering, University of California at San Diego, 9500 Gilman Dr., La Jolla, CA 92093, USA
[d]Mechanical and Aerospace Engineering, University of California at San Diego, 9500 Gilman Dr., La Jolla, CA 92093, USA

Abstract
A new fabrication technique is devised to synthesize conformal Si core-shell nanoparticles (NPs) with Si boride nanoshell by reacting the surface atoms of Si NPs (50–200 nm diameter) with a molten salt of sodium borohydride. The shell layer, about 10–20 nm thick, consists of a mixture of crystalline phase (SiB_x) and other amorphous phases as identified by TEM and EELS analysis. New absorbance peaks for Si-Si boride core-shell NPs appear at the wavenumber of 940 and 777–677 cm^{-1} in FT-IR analysis. TGA analysis reveals that the core-shell structured Si-Si boride NPs exhibit a remarkably improved resistance to thermal oxidation by a factor of 4.6 at 750 °C and at by a factor of 3.5 at 850 °C compared to bare Si. Optical measurements show that spectrally selective coating (SSC) layers made of Si-Si boride NPs have a superior optical stability to that of the bare Si NPs after annealing at high temperature, and desirably exhibit a lower reflectance in the visible spectrum range than the bare Si NPs. These surface-protected, oxidation-resistant semiconductor materials and their novel fabrication methods exhibit further broad applicability of boride nanolayers which can be used for high temperature applications such as solar thermal power generation.
© 2014 Elsevier Ltd. All rights reserved.

*Corresponding author at: Mechanical and Aerospace Engineering, University of California at San Diego, 9500 Gilman Dr., La Jolla, CA 92093, USA.
E-mail address: jin@ucsd.edu (S. Jin).

Introduction

High performance semiconductor materials and metals have been required to develop for various cutting-edge applications including solar power systems, photoelectrochemical hydrogen generation systems, aerospace systems, and microelectronics [1-7]. Some of these applications involve high temperature operation, for instance, in solar thermal applications and aerospace systems. Especially, for solar absorbers in concentrating solar power (CSP) systems, it has been tried to find metals and semiconductor materials stable at high operation temperature which enables to achieve higher thermal efficiency due to Carnot cycle type processes involved [2]. As recently demonstrated, concentrating solar thermoelectric generator (CSTEG) also needs to make high temperature condition made by the absorbed sunlight to obtain better efficiency [8-10].

However, a high temperature operation of metals and semiconductor materials in air atmosphere can cause significant oxidation and the degradation of device performance. For instance, one of important semiconductor materials, silicon, grows a 32 nm-thick oxide layer after annealing for 50 h at 700 °C in dry oxygen [11]. Smaller particle sizes such as nanoparticles are desirable for enhanced sunlight absorption, but smaller particles are more susceptible to oxidation, especially at higher temperatures. Therefore, high performance materials resistant to thermal oxidation is necessary to be developed for the operation in air at elevated temperature, to achieve stable performance of systems.

The objective of this research is to design new types of surface-protected Si nanoparticles with improved oxidation resistance by means of a novel nanoshell-synthesizing method, which can be a prototype of oxidation-resistant core-shell nanoparticles used for the power system operated at high temperature. One candidate material for the passivation nanolayer is boride alloys which have been studied to apply for high temperature applications including a nuclear reactor and aerospace systems because of their good properties in the aspect of melting temperature, hardness, thermal shock resistance and oxidation resistance [12-14]. For this research, Si boride nanoshell was employed to make conformal coating on the surface of Si nanoparticles because Si borides such as β-SiB_3 are known to exhibit superior resistance to thermal oxidation up to 1000 °C in air [15]. In addition, vitreous coatings as a tightly sealed anti-oxidation layer was also investigated to increase the oxidation resistance [16-19].

Silicon borides have been made by a few different kinds of method including fusion, sintering, reduction, chemical vapor deposition (CVD), and e-beam evaporation which synthesized ingot form and thin film of silicon borides [20-26]. But these procedures for making Si-B alloys is difficult to be applied for the fabrication of a conformal Si boride nanoshell on the surface of Si nanoparticles because fusion and sintering process is proper for large-sized ingot and CVD or e-beam evaporation is the more appropriate method for forming thin films on substrates.

We have therefore designed a novel process to create a conformal Si boride shell on the surface of Si nanoparticles, utilizing a molten salt of sodium borohydride ($NaBH_4$) as a boron source. Using this strategy, we have successfully fabricated such a protective boride nanolayer on Si nanoparticles, characterized the coated layer, and discussed its impact on oxidation resistance as well as optical reflection behavior.

Materials and methods

Synthesis of Si boride nanoshell on the surface of Si nanoparticles

Si nanoparticles (∼99.9% purity) with average particle size of 100 nm as a core material and $NaBH_4$ (∼98% purity) powder as a boron source were purchased from Alfa Aesar (Ward Hill, MA). For sample preparations, the Si nanoparticles and $NaBH_4$ powder were thoroughly mixed together by repeated grinding with a mortar and a pestle in a globe box under Ar atmosphere. A quartz tube was sealed with the mixed powders and Ar gas, and heat-treated at 500 °C for 2 days which enabled $NaBH_4$ in the form of a molten salt to make a diffusional reaction with the surface atoms of Si nanoparticles to form a Si boride shell. After the reaction, the residual unreacted $NaBH_4$ was dissolved away with de-ionized (DI) water, and the core-shell nanoparticles were collected with a centrifuge followed by freeze-drying. To crystallize Si boride nanoshell, an annealing process of 900 °C/5 h under Ar atmosphere was employed. After annealing, some portion of the shell remained amorphous. An additional shell-passivation process was applied at 550 °C for 1 h in an oxidizing atmosphere of air in order to convert the amorphous phase in the shell to a passivating borate phase (presumably a glassy borosilicate phase that would not oxidize further) as a part of the shell structure. Without this stabilizing heat treatment step, the oxidation resistance was inferior on high temperature exposure, which was observed with weight gain by thermo-gravimetric analysis (TGA). For the comparative phase analysis, SiB_3 particles, and SiB_6 particles were prepared by ball-milling of arc-melted metal ingots with the same stoichiometric compositions.

Characterization of core-shell structure

The core-shell structure of the as-made Si-Si boride NPs was imaged with transmission electron microscope (TEM) (FEI Tecnai F30G2 Polara) operated at 300 kV in bright field (BF) mode and high resolution (HR) mode, as shown in Figure 1(a). The scanning electron microscope (SEM) analysis was also carried out with the microstructure shown in Figure 1(b). The crystal structure of Si boride shell was analyzed after the annealing and shell-passivation procedure with TEM and a fast Fourier transform (FFT) analysis (see Figure 2).

The presence of boron in the shell layer of Si-Si boride NPs was confirmed by electron energy loss spectroscopy (EELS) with an approximate boron content estimated. For EELS analysis, the sample was imaged with TEM (FEI Tecnai TF-20 FEG) operated at 200 kV in high-angle annular dark-field (HAADF) scanning transmission electron microscope (STEM) mode. EELS line scanning was made in STEM mode using a nominal 1 nm electron beam and a Gatan Enfina DigiPEELS spectrometer (see Figure 3).
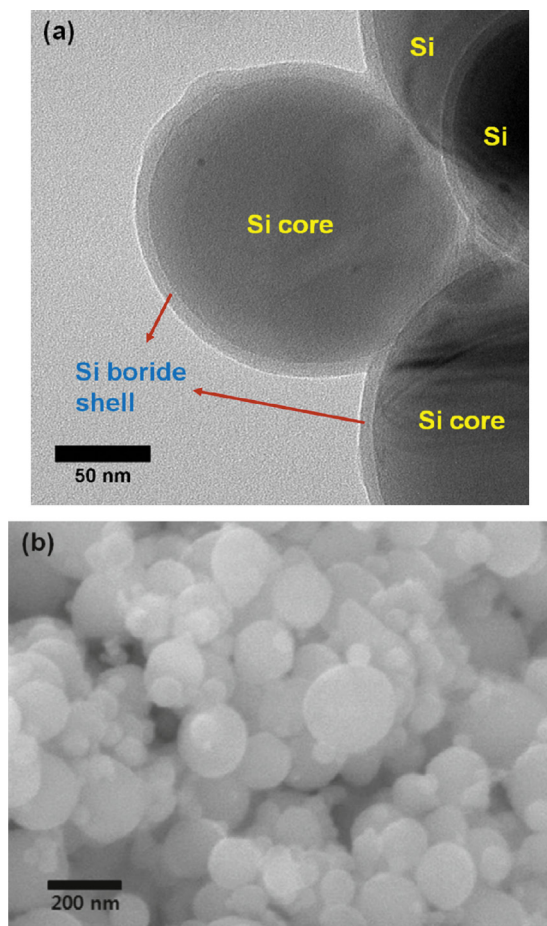
Figure 1 Microstructural images of as-made Si–Si boride core–shell nanoparticles; (a) TEM image showing 10-20 nm thick Si boride shell, and (b) lower mag SEM image of overall core-shell nanoparticles.

FT-IR analysis

For the annealed Si–Si boride NPs and bare Si NPs, infrared absorbance measurement was performed using Fourier transform infrared spectroscopy (FT-IR) (Nicolet 6700 analytical MCT FT-IR Spectrometer) to observe the effect of Si boride shell on the IR absorbance behavior. And FT-IR analysis was also made for ball-milled SiB_3, and SiB_6 particles to be compared to Si–Si boride NPs. The spectrum was scanned with the data spacing of $0.4\,cm^{-1}$.

Analysis of thermal oxidation resistance

For the Si–Si boride NPs, the thermal oxidation resistance was evaluated by measuring the total weight gain of particles during heating in a pure oxygen atmosphere with thermo-gravimetric analysis (TGA). Measurements were carried out at two different holding temperatures of $750\,°C$ and $850\,°C$. Samples were heated at a rate of $20\,°C/min$ to the maximum temperatures and held there for 2 h.

Optical reflectance measurement of SSC layers

To compare optical reflectance of Si boride-coated Si NPs with bare Si NPs, spectrally selective coating (SSC) layers were prepared by drop-casting the prepared nanoparticles dispersed in ethanol onto Inconel® 625 super alloy substrates, which are commonly used for metal tubes carrying heat transfer fluids inside and coated with the solar absorber materials outside the tubing in concentrating solar power systems. The thickness of the SSC layers made of the prepared nanoparticles was ~100 μm and the area of the coated region was 1 cm². Visible/IR reflectance of SSC layers was measured, using a home-made optical measurement system consisting of an integration sphere (4″ Lab-Sphere®, Spectraflect® coated) assembled with an Andor® Shamrock 303i spectrometer equipped with Si and InGaAs-based detectors. The reflectance was measured with incidence angle of 12.5° in the spectrum range of 400-2000 nm at room temperature. In order to observe the effect of Si boride nanoshell on the stability of optical property at high temperature, the reflectance of SSC layers was also measured after both bare Si and Si–Si boride NPs were annealed at 850 °C for 5 h and 10 h in air.

Results and discussion

Shell formation and composition of Si–Si boride core-shell NPs

Sodium borohydride ($NaBH_4$) powder material starts to melt at 400 °C to form a molten salt of Na^+ $[BH_4]^-$ [27], followed by decomposition reactions at 450 °C into $[NaH+B+1.5H_2]$ or $[Na+B+2H_2]$ [28]. During the shell-forming procedure occurring when the temperature reaches 500 °C, phases such as a molten salt phase, a decomposed gas phase (H_2) and solid phases can coexist. In this mixed-phase state at 500 °C, boron atoms from $NaBH_4$ can diffuse and react with Si atoms to form a desirable Si boride nanoshell on the surface of Si nanoparticles, which can serve as an oxidation-resistant protective layer.

Various structural and compositional analyses of the $NaBH_4$-reacted Si nanoparticles were performed using SEM, TEM, EELS and FT-IR. The microstructures of as-made, core–shell nanoparticles of Si–Si boride are shown in Figure 1. The TEM image, Figure 1(a), clearly indicates the core-shell configuration with Si core (~150 nm diameter) and a well defined and conformal Si boride shell (10-20 nm). The overall morphology and size distribution of Si boride-coated Si nanoparticles are depicted in the SEM image of Figure 1(b), which shows some distribution of the particle diameter of 50-200 nm, arising from the size distribution of the starting Si nanoparticles.

Shown in Figure 2 are TEM micrograph (Figure 2(a)) and the corresponding FFT pattern (Figure 2(b)) for the core-shell NPs with the annealed and passivated Si boride shell. The core is a polycrystalline silicon which is represented by main (111) crystal structure with P1 pattern as well as other crystalline structures such as Si (311) with P4 pattern, as shown in Figure 2(b). The shell is composed of the mixture of some crystalline phases (the inset in Figure 2(a)) including Si boride (P2, and P3 patterns in Figure 2(b)) and some
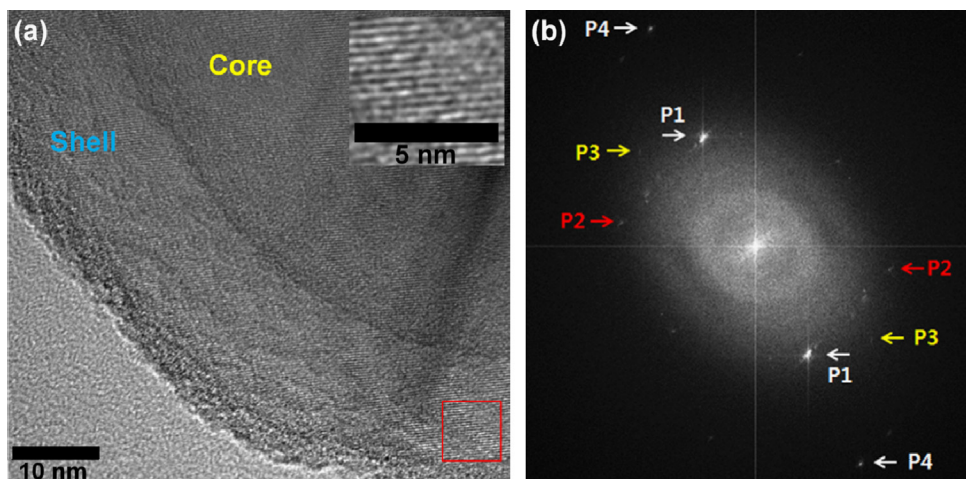
Figure 2 (a) TEM image near the shell area of a Si–Si boride core-shell nanoparticle with the inset showing the lattice image taken from red-lined square area in the shell area (lower right in Figure 2(a)), and (b) corresponding FFT patterns for the image (a) showing some crystal phases (P2, P3 in (b)).

Table 1 Summary table for the possible crystal structures for core and shell calculated from the FFT patterns in Figure 2(b).

	FFT patterns	d-spacing	Crystal structures
Core (Si)	P1	3.1755 Å	Si(111)
	P4	1.5983 Å	Si(311)
Shell (Si boride)	P2	2.8142 Å	SiB_3(104), SiB_6(260), SiB_6(351)
	P3	2.5633 Å	SiB_3(113), SiB_3(202), SiB_6(162), SiB_6(450)

amorphous phases including Si–B amorphous phase, borosilicate and silica which was formed during the annealing and shell-passivation procedure. The P2 pattern in Figure 2(b) has d-spacing of 2.8142 Å which corresponds to the d-spacings of SiB_3 (104), SiB_6 (260), or SiB_6 (351) as summarized in the Table 1. Another crystalline pattern, P3 in Figure 2(b) has d-spacing of 2.5633 Å which is close to the d-spacings of SiB_3 (113), SiB_3 (202), SiB_6 (162) or SiB_6 (450).

EELS analysis was utilized to confirm the existence of boron as well as the composition in the shell of the core-shell nanoparticles. The diameter of Si–Si boride NP analyzed by EELS was approximately 80 nm in STEM image as indicated in Figure 3(a) where the shell thickness of the core-shell particle was about 10 nm. The line scanning of EELS analysis was made for the region along 28 nm length along the direction from the core side (the core covered with shell) to the shell side (near the edge of the particle). Through this line-scanning in STEM mode, EELS spectrum could be measured for each Si and B, as shown in Figure 3(b). Line [I] in Figure 3(b) and (c) indicates the boundary between the shell-coated core region (the left side of line [I]) and pure shell region (the right side of line [I]). For the line scanning of the core part (the left side of line [I] in Figure 3(b)), the electron beam passes the top shell, Si core, and bottom shell of the spherical particle in that order. For the line scanning of the shell part (the right side of line [I] in Figure 3(b)), the beam goes through only the shell with progressively less material scanned as the beam moves out to the edge of the spherical particle.

The fractional compositions of core and shell in Si–Si boride NP were calculated (Figure 3(c)) using the EELS spectrum which had the counts of energy loss signal for every 1 nm step (Figure 3(b)). After a single spectrum (60–725 eV) was acquired at every 1 nm, the many spectra were then converted into a line scan graph. The principal edge values of energy loss for each element, 99 eV and 188 eV were used to measure signals of Si and B element, respectively. The shell part is detected approximately from 17 nm to 28 nm on the Line Scan axis in Figure 3(b) and (c), if considering both STEM image and EELS spectrum. The core part is thought to be from 0 nm to 17 nm on the Line Scan axis, where both core material (Si) and shell materials (Si, and Si boride) exist.

It can be estimated from Figure 3(c) that the atom ratio of Si/B in the shell part is 5/1–30/1, which means that B content is a smaller amount than Si in the overall area of the shell. In the phase diagram of Si–B alloy, the alloy with Si/B atom composition of 5/1–30/1 is composed of two phases including Si and SiB_3 [29]. Therefore, the shell of the annealed Si–Si boride NPs is thought to consist of binary phases including crystalline SiB_3 phase and Si phase except amorphous phases as observed in TEM image and FFT pattern of Figure 2.

Effect of Si boride shell on the absorbance of IR spectrum

FT-IR measurement was made for the annealed Si–Si boride NPs and bare Si NPs in order to compare infrared (IR)

absorbance behaviors of these two types of particles in relation with the effect of Si boride shell. Bare Si particles have the strong absorbance peaks in the region of
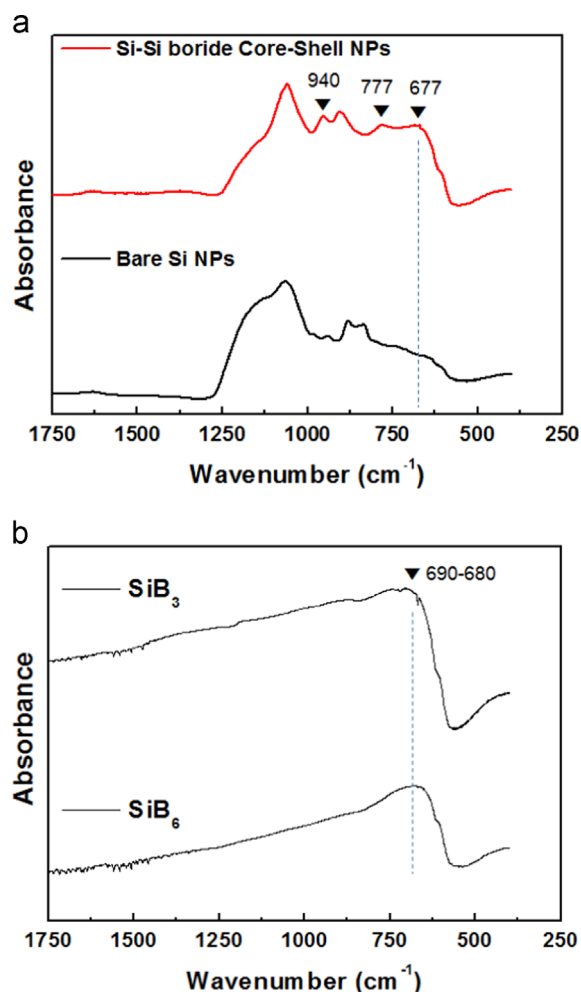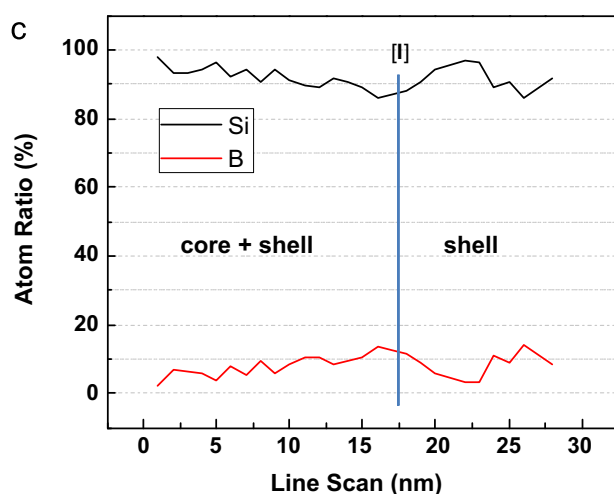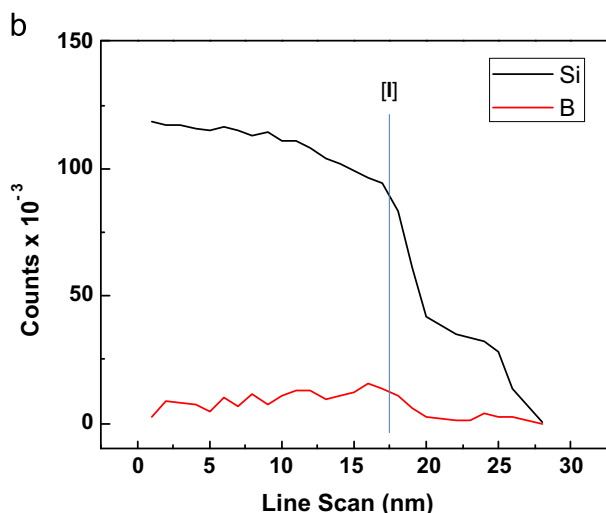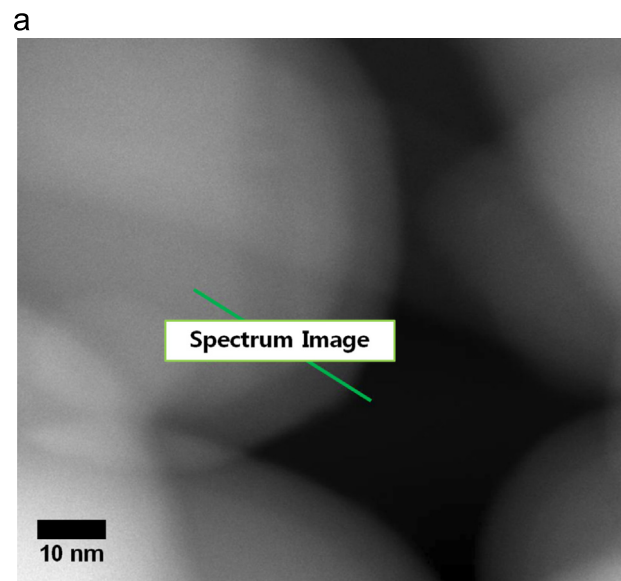

Figure 4 FT-IR analysis showing (a) Si-Si boride NPs have new absorbance peaks containing a broad band with two peaks of 777-677 cm^{-1} and another peak of 940 cm^{-1} compared to bare Si NPs, and (b) the main absorbance is made at 690-680 cm^{-1} for SiB$_3$, and SiB$_6$ material.

1100-1000 cm^{-1} and 880-834 cm^{-1}, as shown in Figure 4(a). The absorbance peak of 1100-1000 cm^{-1} was reported for the vibration of Si-O bonding and the peak of 880-834 cm^{-1} results from the vibration of O-Si-O bonding [30]. The synthesized core-shell NPs display a new absorbance peak at 940 cm^{-1} and a new broad band composed of two peaks in the region of 777-677 cm^{-1}, which are expected to be affected by boron-containing bonds of the Si boride shell formed by the diffusion of boron atoms into Si surface based on the following analysis.

As illustrated in Figure 4(b), the SiB$_3$ and SiB$_6$ particles have the main absorbance peaks in the range of 690-680 cm^{-1}. The vibration band for B–B bonding was reported to oc-cur ap-pr-oxi-ma-tely

Figure 3 (a) STEM image showing the line-scan part (green line, spectrum image) of EELS in the core-shell Si-Si boride NPs, (b) EELS spectrum showing the counts of energy loss signal for each element (Si and B) on line-scanning from the core side to the shell side, and (c) the composition of core side and shell side in Si-Si boride core-shell nanoparticle, calculated from the EELS spectrum.

in the range of 1100-600 cm^{-1} [31]. One absorbance peak (677 cm^{-1}) of the broad band (777-677 cm^{-1}) for Si-Si boride NPs matches with the main absorbance peaks of SiB$_3$ (690-680 cm^{-1}) and SiB$_6$ (690-680 cm^{-1}) particles. Si-O-B bonding was reported to have the absorbance peak in two wavenumbers of 930 and 680 cm^{-1} [30], which seems to represent a similar absorption behavior to that of the Si-Si boride NPs with the absorbance peaks (940 cm^{-1} and 677 cm^{-1} in Figure 4(a)). Also, B-O bonding was reported to make an absorption at the wavenumber of 1400 cm^{-1} [30], where the synthesized Si-Si boride NPs show the broad and weak absorbance peak, as can be seen in Figure 4(a). Based on this FT-IR analysis, it can be concluded that the new absorbance peaks of Si-Si boride NPs result from the formation of Si boride shell which is composed of boron-reacted materials including the forms of Si-B alloy (Si boride), and SiO$_2$-B$_2$O$_3$ (borosilicate).

Improved resistance to thermal oxidation

The thermal oxidation resistance was measured with TGA in a pure oxygen atmosphere for Si-Si boride nanoparticles. The total weight gain of particles resulting from the thermal oxidation was compared to that of bare Si nanoparticles. We utilized accelerated oxidation method by using pure oxygen atmosphere at high temperatures.

Shown in Figure 5 are the comparative TGA analysis data showing the enhanced thermal oxidation resistance of the Si-Si boride core-shell NPs compared to the bare Si NPs. Thermal oxidation was measured based on the weight change of TGA during a temperature increasing step and a temperature holding step at 750 °C (Figure 5(a)) and 850 °C (Figure 5(b)). These accelerated oxidation tests in pure oxygen atmosphere by TGA indicate that the core-shell Si-Si boride NPs with boron-alloyed shells exhibit a much higher resistance to thermal oxidation than bare Si NPs. After holding at 750 °C for 2 h in TGA test, the core-shell NPs had a much smaller amount of weight gain (3.2 wt%) by a factor of 4.6 compared to that of bare Si NPs (14.6 wt%). Similarly as for the 750 °C TGA, the 850 °C TGA results also indicate that the weight gain (9.4 wt%) of the core-shell nanoparticles decreased much by a factor of 3.5 in comparison to bare Si NPs (33 wt%), after the temperature holding step of 850 °C/2 h.

This significantly enhanced oxidation resistance of the core-shell structured Si-Si boride NPs results from the contribution of the conformally present shell layer which consists of crystalline Si borides (SiB$_3$, or SiB$_6$) and other vitreous phases including borosilicate. From the previously reported researches, it can be expected that crystalline β-SiB$_3$ [15], and vitreous borosilicate layer [16-19] helps to decrease oxidation rate. The reduced oxidation data clearly indicates that the oxygen diffusion through the Si boride shell layer in the core-shell NPs is significantly slower than through the pure Si material.

Optical properties of SSC layers

High temperature applications of semiconductors are receiving more attention these days, for example, more efficient solar cells and thermoelectric devices using concentrated/
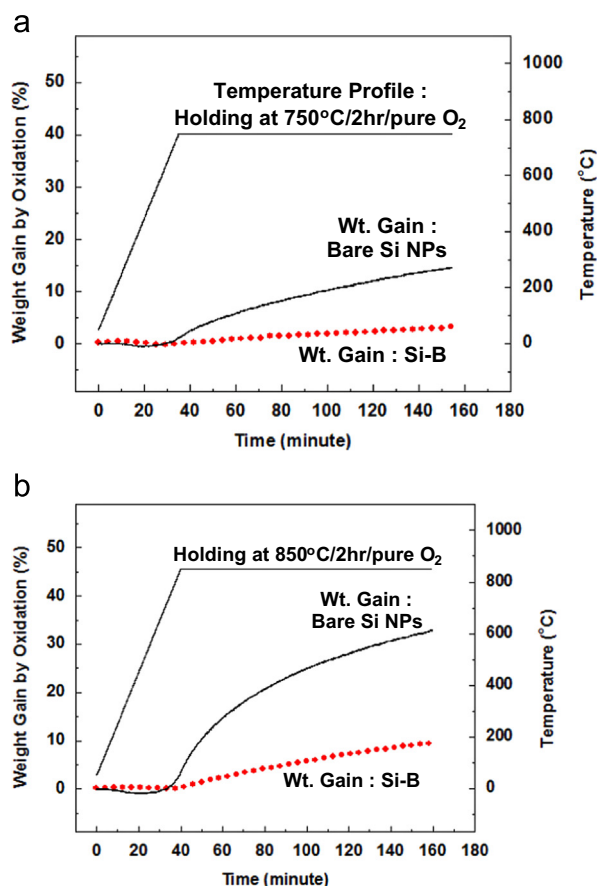

Figure 5 Accelerated TGA analysis comparing bare Si nanoparticles to the surface-protected, core-shell structured Si-Si boride nanoparticles (Si-B), (a) at 750 °C, and (b) at 850 °C in pure oxygen atmosphere.

focused sunlight with the naturally higher operating temperatures [8-10]. Therefore, high temperature oxidation resistant coating on a semiconductor surface is generally desirable. While the main focus of this research is on the improved oxidation resistance of Si based semiconductor nanomaterials at high temperatures for potential applications to a variety of devices, one example of the such possible applications of the surface-protected Si nanoparticles is for efficient sunlight absorption in the Concentrating Solar Power (CSP) power generating system. Therefore, the optical reflection measurement was made on SSC layers composed of Si-Si boride NPs coated on Inconel substrate and exposed to high temperatures, as compared to bare Si NPs processed in a similar manner.

The reflection measurement was made with the form of spectrally selective coating (SSC) layer composed of Si-Si boride NPs and another Si NPs casted on Inconel substrate as shown in Figure 6 in order to compare the thermal stability of optical property based on the reflection measurement with annealing at high temperature in air atmosphere.

As can be seen in Figure 6, the prepared SSC layers with Si-Si boride NPs exhibits very little change in the surface color from the initial dark brown for as-prepared sample even after they were exposed to 850 °C annealing for 10 h in air. This implies that the Si-Si boride NPs can provide a
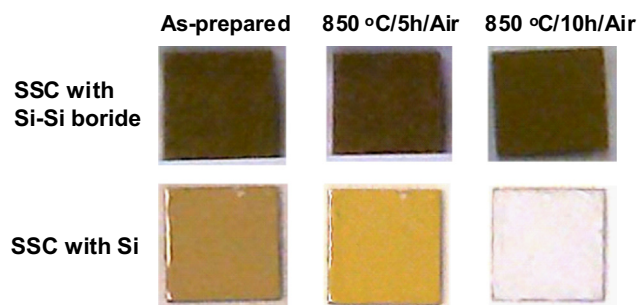
Figure 6 Surface color change of SSC layers after annealing at 850 °C with the high temperature exposing time increasing up to 10 h under air atmosphere.

strong resistance to thermal oxidation. On the contrary, SSC layers made of bare Si NPs have quite an obvious change of surface color from the initial light brown to orange color when exposed to 850 °C for 5 h, then to nearly white color after exposure to 850 °C for 10 h (Figure 6). These changes to lighter colors are caused by easy oxidation of bare Si NPs at high temperature in air.

Figure 7 shows the comparison of the optical reflectance between the SSC layer of Si–Si boride NPs and that of Si NPs. As shown in Figure 7(a), from long to short wavelengths, the reflectance starts decreasing abruptly at the wavelength of 1.05–1.08 μm, corresponding to bandgap of Si (1.13 μm or 1.12 eV) [32], and continues to reduce more gradually to 400 nm in the visible spectrum. If the transition point of reflectance is defined as the cut-off wavelength of reflection, it can be analyzed from Figure 7(a) that the cut-off point of SSC layers with Si–Si boride NPs remains stable near the wavelength regime of 1.05–1.08 μm μm even though the reflectance in the near-IR regime was somewhat affected by the high temperature exposure, with the reflectance after 10 h exposure at 850 °C stabilizing toward the original value in the as-made samples (further research is required for understanding of specific effects of high temperature annealing parameters). Compared to the stable cut-off wavelength behavior of the SSC layer comprising the surface-protected Si NPs, the SSC layer with bare Si NPs exhibits a profound change upon 850 °C exposure, with the cut-off wavelength becoming significantly shorter from 1.05–1.08 um in the near IR regime to 645 nm in the visible spectrum regime as shown in Figure 7(b). After annealing at 850 °C, the reflectance of visible spectrum in SSC layers with Si–Si boride NPs are much more stable than that with bare Si NPs which experiences more increment of reflectance with annealing time increasing as shown in Figure 7(b). This implies that most part of the bare Si NP was transformed into an insulating SiO_2 phase upon exposure to 850 °C for 10 h in air atmosphere in agreement with the color changes shown in Figure 6.

While further R&D will be required to optimize the surface protection structures and their behavior, the sunlight receiver made of SSC layers with surface-protected Si–Si boride type NPs can be expected to enable a more stable/reliable electricity generation during high temperature operation in various solar thermal applications than with pure surface-unprotected semiconductor materials. Furthermore, the reflectance values in the visible spectrum
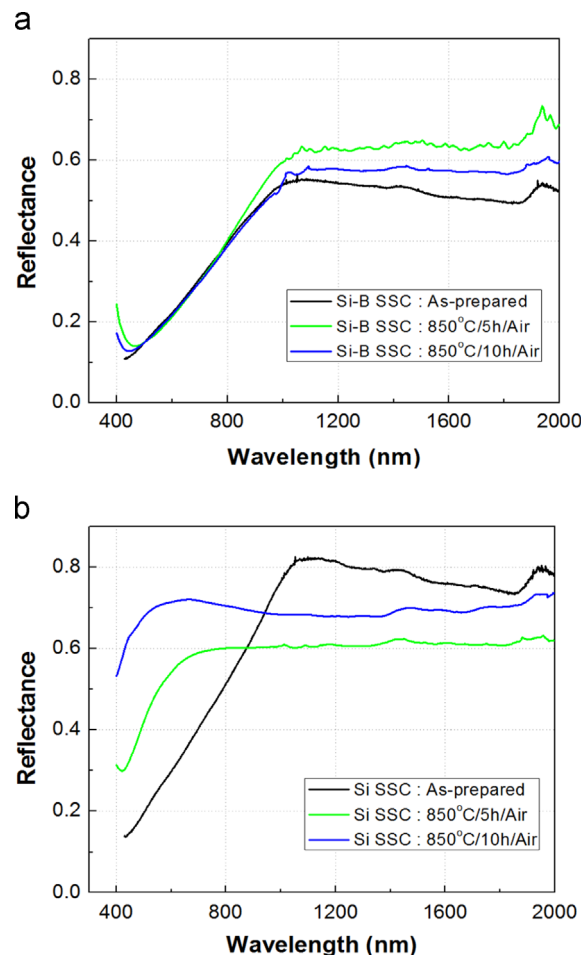

Figure 7 Reflectance measurements of high temperature exposed SSC layers made of (a) Si–Si boride NPs (Si-B), and (b) bare Si NPs.

representing a greater amount of sunlight energy is substantially lower in SSC layers with Si–Si boride NPS than that with bare Si NPs, which also allows much more efficient sunlight absorption so as to reach higher thermal efficiency.

Summary

The present study reports a new fabrication method to make conformal, surface-protecting Si boride nanoshell on Si nanoparticles, and associated microstructural and optical properties. The 10–20 nm thick uniform coating of Si boride shell was formed by reacting surface atoms of Si nanoparticles with a molten salt of sodium borohydride. The presence of the Si boride shell was confirmed by TEM, EELS and FT-IR analyses. Based on the TGA analysis, it was found that the boride-coated core-shell Si nanoparticles exhibit remarkably improved resistance to thermal oxidation by a factor of 4.6 at 750 °C and 3.5 at 850 °C. Optical measurements show that spectrally selective coating (SSC) layer of Si–Si boride NPs has superior optical stability and lower reflectance compared to that of bare Si NPs after exposure to 850 °C annealing, exhibiting a significantly higher

absorption in the visible spectrum range. These surface-protected, oxidation-resistant semiconductor materials and their novel synthesis methods can be useful for various high temperature solar thermal or solar electric applications.

Acknowledgments

References

[1] A. Lenert, D.M. Bierman, Y. Nam, W.R. Chan, I. Celanovic, M. Soljacic, E.N. Wang, Nat. Nanotechnol. 9 (2014) 126-130.

[2] D.E. Carlson, C.R. Wronski, Appl. Phys. Lett. 28 (1976) 671-673.

[3] A.G. Aberle, Prog. Photovolt.: Res. Appl. 8 (2000) 473-487.

[4] R.N. Dominey, N.S. Lewis, J.A. Bruce, D.C. Bookbinder, M.S. Wrighton, J. Am. Chem. Soc. 104 (1982) 467-482.

[5] Y. Cui, Z. Zhong, D. Wang, W.U. Wang, C.M. Lieber, Nano Lett. 3 (2003) 149-152.

[6] G.W. Meethan, J. Mater. Sci. 26 (1991) 853-860.

[7] C.E. Kennedy, Review of Mid to High Temperature Solar Selective Absorber Materials, NREL Technical Report, NREL/TP-520-31267, 2002.

[8] D. Kraemer, B. Poudel, H.-P. Feng, J.C. Caylor, B. Yu, X. Yan, Y. Ma, X. Wang, D. Wang, A. Muto, K. McEnaney, M. Chiesa, Z. Ren, G. Chen, Nat. Mater. 10 (2011) 532-538.

[9] M. Jang, Y. Park, M. Jun, Y. Hyun, S.-J. Choi, T. Zyung, Nanoscale Res. Lett. 5 (2010) 1654-1657.

[10] L.L. Baranowski, G.J. Snyder, E.S. Toberer, Energy Environ. Sci. 5 (2012) 9055-9067.

[11] B.E. Deal, A.S. Grove, J. Appl. Phys. 36 (1965) 3770-3778.

[12] L. Kaufman, in: J.T. Waber, P. Chiotti, W.N. Miner (Eds.), Compounds of Interest in Nuclear Reactor Technology, AIME, New York, 1964, p. 193.

[13] M.M. Opeka, I.G. Talmy, J.A. Zaykoski, J. Mater. Sci. 39 (2004) 5887-5904.

[14] R.G. Munro, J. Res. NIST 105 (2000) 709-720.

[15] J.R. Salvador, D. Bilc, S.D. Mahanti, M.G. Kanatzidis, Angew. Chem. Int. Ed. 42 (2003) 1929-1932.

[16] P.C. Innocenzi, M. Guglielmi, M. Gobbin, P. Colombo, J. Eur. Ceram. Soc. 10 (1992) 431-436.

[17] M. Guglielmi, D. Festa, P.C. Innocenzi, P. Colombo, M. Gobbin, J. Non-Cryst. Solids 147 and 148 (1992) 474-477.

[18] J.A. Lemberg, R.O. Ritchie, Adv. Mater. 24 (2012) 3445-3480.

[19] K. Kobayashi, K. Maeda, H. Sano, Y. Uchiyama, Carbon 33 (1995) 397-403.

[20] H. Moissan, A. Stock, C. R. Acad. Sci.(Paris) 131 (1900) 139.

[21] C.F. Cline, Nature 181 (1958) 476-477.

[22] E. Colton, J. Am. Chem. Soc. 82 (1960) 1002.

[23] C. Brosset, B. Magnusson, Nature 187 (1960) 54-55.

[24] H.F. Rizzo, L.R. Bidwell, J. Am. Ceram. Soc. 43 (1960) 550-552.

[25] T. Goto, M. Mukaida, T. Hirai, Mater. Res. Soc. Symp. Proc. 168 (1990) 167-172.

[26] J.R.A. Carlsson, X.-H. Li, S.F. Gong, H.T.G. Hentzell, J. Appl. Phys. 74 (1993) 891-896.

[27] Y. Filinchuk, A.V. Talyzin, D. Chernyshov, V. Dmitriev, Phys. Rev. B 76 (2007) 092104-1-092104-4.

[28] J. Urgnani, F.J. Torres, M. Palumbo, M. Baricco, Int. J. Hydrog. Energy 33 (2008) 3111-3115.

[29] R.W. Olesinski, G.J. Abbaschian, Bull. Alloy Phase Diagr. 5 (1984) 478-484.

[30] K. Murase, T. Ogino, Y. Mizushima, Jpn. J. Appl. Phys. 22 (1983) 1771-1777.

[31] G.-R. Yang, Y.-P. Zhao, B.Y. Tong, Mater. Res. Soc. Symp. Proc. 426 (1996) 83-88.

[32] S.M. Sze, Physics of Semiconductor Devices, 2nd Ed., Wiley, New York15.

Tae Kyoung Kim is a Ph.D. candidate in the Materials Science and Engineering Program at University of California, San Diego (UCSD). He obtained B.S. and M.S. degree from Yonsei University (South Korea) and had worked at Samsung Cheil Inc. (presently, Samsung SDI) as a senior researcher mainly in the field of materials for renewable energy generation and storage systems. And then he has been studying and researching in UCSD since 2011.
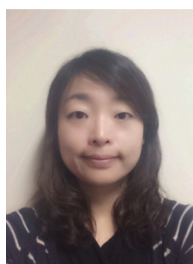
Jaeyun Moon is a Ph.D. candidate in the Materials Science and Engineering Program at University of California, San Diego (UCSD). She obtained her B.S. and M.S. degree from Hanyang University (South Korea) and had worked at Samsung Electronics as a senior engineer and then joined UCSD in 2009 as a research assistant. She has focused on renewable energy generation, especially thermal energy conversion, such as concentrated solar power and thermoelectrics.
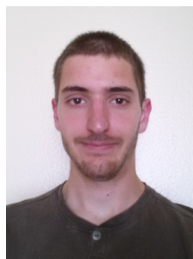
Bryan VanSaders is a Ph.D. graduate student in the Material Science and Engineering department at University of California, San Diego (UCSD). He obtained his B.S. degree from Rutgers University and M.S. degree from UCSD. He has focused on nano-scale optics, plasmonics, and optical metamaterials.

Dongwon Chun is a Ph.D. student in the Materials Science and Engineering Program at University of California, San Diego (UCSD) since 2012. He obtained B.S. and M.S. degree from Yonsei University (South Korea) and had worked at the Korea Institute of Science and Technology as a research scientist mainly working on the Bio-MEMs and Materials Analysis.

Calvin Gardner is a Ph.D. candidate in the Mechanical and Aerospace Engineering Program at University of California, San Diego (UCSD). He received his M.S. degree from UCSD in Engineering Physics and a B.S. degree in Mechanical Engineering, Applied Physics, and Philosophy from Brigham Young University. His main research interests focus on the application of advanced material processing techniques to specific product designs.
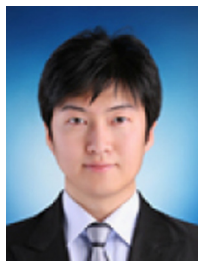
Jae-Young Jung is a Ph.D. student in the Materials Science and Engineering Program at University of California, San Diego (UCSD). He graduated from Dankook University in South Korea in 2006 (B.S.) and 2008 (M.S.). He has three years of working experience at U&i Corporation (South Korea) and two years at the Korea Institute of Science and Technology in the field of medical device and biomaterials analysis of by using electron microscopy. He is now actively working in the area of the analysis of biomaterials and the development of bioinspired materials in UCSD since 2013.
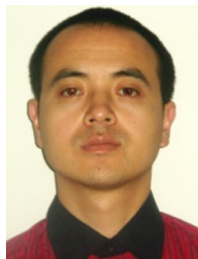
Gang Wang obtained his Ph.D. from Department of Chemistry at Syracuse in 2011. His research interest focus on the silica nanoporous materials preparation and their application in drug delivery and catalyst. He obtained B.S. from Zhengzhou University and M.S. degree from Lanzhou Institute of Chemical Physics, Chinese Academy of Sciences.

Renkun Chen received his B.S. degree in Thermo-physics from Tsinghua University in 2004, and a Ph.D. degree in Mechanical Engineering from University of California, Berkeley in 2008. Following a one-year stint as a postdoctoral fellow at Lawrence Berkeley National Laboratory, he joined University of California, San Diego as an Assistant Professor in the Department of Mechanical and Aerospace Engineering in 2009. His research interests include nanoscale heat transfer, energy conversion materials, and thermal management.

Zhaowei Liu is an Assistant Professor of Electrical and Computer Engineering at University of California, San diego (UCSD). He received his Ph.D. in mechanical engineering (MEMS/Nanotechnology) from University of California, Los Angeles in 2006. Before joining UCSD faculty, he was a postdoctoral researcher at the NSF Nanoscale Science & Engineering Center (NSEC) in the Mechanical Engineering Department at University of California, Berkeley. His research interest include nanophotonics, plasmonics, metamaterials, energy and ultrafast opto-electronics.

Yu Qiao is a Professor in the Program of Materials Science & Engineering and the Department of Structural Engineering at University of California, San Diego. Professor Qiao received his Ph.D. degree in Mechanical Engineering from the Massachusetts Institute of Technology in 2002. His research interests include advanced battery materials, advanced protective materials and structures, space infrastructural materials, energy conversion for low-grade heat, and failure analysis of engineering materials.

Sungho Jin received his B.S. degree in Metallurgical Engineering from Seoul National University in 1969, and Ph.D. degree in Materials Science & Engineering from University of California, Berkeley in 1974. After 26 years of R&D at Bell Laboratories at Murray Hill, New Jersey, he joined University of California, San Diego (UCSD) in 2002 as a Professor and Iwama Endowed Chair. He is currently a Distinguished Professor at UCSD, and is serving as the Director of UCSD-wide Materials Science & Engineering Program. His research interests include R&D of nano materials, magnetic materials, electronic materials, energy materials, and bio materials.